Available online at www.sciencedirect.com
SCIENCE DIRECT®
International Journal of Mass Spectrometry 244 (2005) 135–143
International Journal of Mass Spectrometry
www.elsevier.com/locate/ijms

SIMION analysis of a high performance linear accumulation octopole with enhanced ejection capabilities

Ioana M. Taban, Liam A. McDonnell, Andreas Römpp, Iliya Cerjak, Ron M.A. Heeren *

FOM Institute for Atomic and Molecular Physics, Kruislaan 407, 1098 SJ Amsterdam, The Netherlands

Received 17 March 2005; accepted 20 May 2005
Available online 5 July 2005

Abstract

Here, we present the results of extensive SIMION 7.0 modelling of a new linear octopole ion trap. The octopole was designed to increase the efficiency of an electrospray ion source coupled to a Fourier Transform Ion Cyclotron Resonance (FTICR) mass spectrometer. This improvement was achieved by applying a pulsed axial field to the octopole to eject the ion packet with a time and energy distribution that better match the acceptance criteria of the FTICR cell, thus increasing the trapping efficiency and sensitivity. The axial field was produced by applying a pulsed dc potential to the custom-designed ejection electrodes located between the octopole rods. The time and energy profiles of the ejected ion packets for several electrode shapes were calculated and are discussed in terms of their compatibility with efficient trapping of the ion packet in the FTICR cell. Preliminary experimental results show increased signal using the dc ejection electrodes of approximately 100%.

Keywords: Linear ion trap; Octopole; FTICR; Simulations; Ejection electrodes

1. Introduction

The application of high performance mass spectrometric methods for biomedical analysis has increasing requirements for sensitivity. Often studies involve the analysis of low copy number molecules in a pool of high abundant proteins [1–4]. Chromatographic separation [3,5], capillary isoelectric focussing [6], and capillary electrophoresis [1] have all been used to reduce the complexity of the samples entering the mass spectrometer at any specific time and to concentrate each analyte. Such hyphenated experiments now permit attomole measurements. However, there are still applications where increased sensitivity is desired. High-throughput proteomics applications and specifically the search for biomarkers (up- and down-regulated proteins, post-translation modifications and point-mutations have all been associated with disease) would benefit from increased sensitivity and a higher dynamic range.

Fourier Transform Ion Cyclotron Resonance Mass Spectrometry (FTICR-MS) is an ion trapping technique [7] that distinguishes itself from other types of mass spectrometry: high spectral resolution, for example resolving two peptides that differ in mass by less than the mass of a single electron [8], and high mass accuracy make the FTICR ideally suited for rapid analysis of complex mixtures [1,4,9]. To be compatible with fast separation techniques the ions must be trapped in the FTICR cell preferably without using a trapping gas. The acceptance criteria for the FTICR infinity cell [10] for non gas-assisted trapping with sidekick are: a trapping time window within 0.2–0.4 ms and kinetic energies of ions lower than 2 eV per charge, for ions with m/z lower than 2000 [11].

The sensitivity of an FTICR experiment is influenced by many factors, including efficiency of ion generation, ion-transport and ion detection. Improvements in all aspects continue unabated [12,13]. Collisional cooling of ion beams in 2D-multipoles, operated in an rf-only mode, have improved the performance of FTICR mass spectrometers and are now widely used in all types of mass

* Corresponding author. Tel.: +31 20 6081234; fax: +31 20 6684106.
E-mail address: heeren@amolf.nl (R.M.A. Heeren).

1387-3806/$ – see front matter © 2005 Elsevier B.V. All rights reserved.
doi:10.1016/j.ijms.2005.05.004

spectrometer [14–17]. Through collisions, the buffer gas reduces the kinetic energy of a particle beam and focuses it on the longitudinal axis of the guiding multipole. This low-energy ion beam can then be focused and transported with high efficiency into the next region of the instrument. It has been shown that if ions are kinetically cooled and accumulated before being pulsed out of the multipole, sensitivity and dynamic range of the experiments are increased [13,16].

However, there is still scope for improving the performance of these linear ion traps. When many ions are present in a linear ion trap, the sensitivity of the measurement can decrease. Space-charge-induced ion discrimination in the multipole can lead to the absence of many expected analyte peaks [18] and multipole storage assisted dissociation (MSAD; space-charge-induced collision-activated dissociation inside the multipole) can lead to fragmentation of the ions of interest [19,20]. Furthermore, the trapping capability of linear ion traps is worse for native bio-macromolecules and their complexes, because their native conformations have smaller collision cross-sections than their de-natured analogues [21]. Though improved trapping has been achieved using increased collision-gas pressure, this causes MSAD to be more problematic [19].

A longer linear multipole ion-trap would alleviate many of the above problems: in a large ion-trap space charge effects occur at larger ion numbers, so the potential for MSAD and ion-discrimination is reduced, and non-covalent complexes have more time to collisionally cool, thus a greater fraction can be trapped. One drawback of a longer trap is that the time distribution of the ejected ions is larger because it takes a longer time for ions located at the beginning of the multipole to move to the end where they can experience the ejection field supplied by the exit lens (during accumulation this lens provides a trapping field). Longer multipoles can lead to lower sensitivity since only a small fraction of the ions accumulated in the multipole are trapped in the FTICR cell. Normally, the multipole length is chosen as a compromise between the ejection time distribution and space-charge considerations.

The time-distribution of the ejected ion packet can be shortened by creating an axial field in the multipole [22]. This would allow the analyst to benefit from the advantages of a longer multipole outlined above. An axial ejection field can be created in several ways without significantly affecting the rf multipole field. Any perturbation of the rf field can reduce the *m*/*z* transmission window. The methods that have been used to date are:

- Segmented multipole rods—by applying a different dc bias to each segment an ejection field can be created with minimal rf-field distortion [23]. In practice, however, because alignment of the segments is key to the design, engineering must be meticulous.
- A set of rings surrounding the multipole—by applying different dc potentials to these rings, an axial field is created with low distortion of the rf field. This design is robust. However, the dc potentials that must be applied to the rings are prohibitively high [24,14].
- Tilted or conical multipole rods—perturbs the rf trapping field making trapping of the incoming ions in the multipole less efficient [24,25].
- Tilted dc wires located inside an octopole [26]—do not affect the rf field significantly, but these wires must be thin making the construction quite fragile and difficult to shape.
- T-shaped electrodes located between quadrupole rods [22]—in this case, four extra electrodes (T-shaped) were placed between the quadrupole electrodes, to which the same dc ejection voltage is applied. By shaping these electrodes, a linear axial field was created through the quadrupole. The setup is simple and the field distortion small.

To increase the efficiency of external accumulation for large ions and to minimize detrimental space-charge-induced artifacts such as MSAD and space-charge induced discrimination, we designed an elongated linear octopole ion trap. To ensure efficient ejection from the octopole, efficient transfer to, and trapping in the ICR cell we added eight T-shaped ejection electrodes, located between the octopole rods, to create an axial field. Extensive simulations were conducted to optimise the time and energy distributions of the ions ejected from the octopole to match the trapping characteristics of the FTICR cell.

2. Description of the simulated accumulation octopoles

The octopole will be used to accumulate ions generated by electrospray ionisation [27], and matrix-assisted laser desorption/ionisation [28]. Consequently, ions covering a wide range of *m*/*z* need to be accumulated, a task best suited to a higher order multipole [29]. The wider *m*/*z* range and higher charge capacity of the octopole compared to that of lower order multipoles (e.g., twice higher than a quadrupole [30]) led to the decision to base our ion trap on an octopole. To increase the multipole order above eight does not yield improvements in performance that would justify the technological complications needed for its realization [31]. To our knowledge this is the first time a linear octopole ion trap equipped with shaped, non-linear, ejection electrodes is considered to enhance the sensitivity of the source of an FTICR-MS.

The octopole is 180 mm long, made of eight circular rods of 6 mm diameter. The field radius of the octopole was chosen such that the ratio $r_{rod}/r_0 = 0.355$. This ratio has been shown to be a good approximation for the ideal octopole field [32]. To maximize the fraction of ions trapped in the linear octopole, the beginning of the octopole was beveled so that octopole fits inside the skimmer of the electrospray ion source. The skimmer and a single electrostatic lens at the end of the octopole

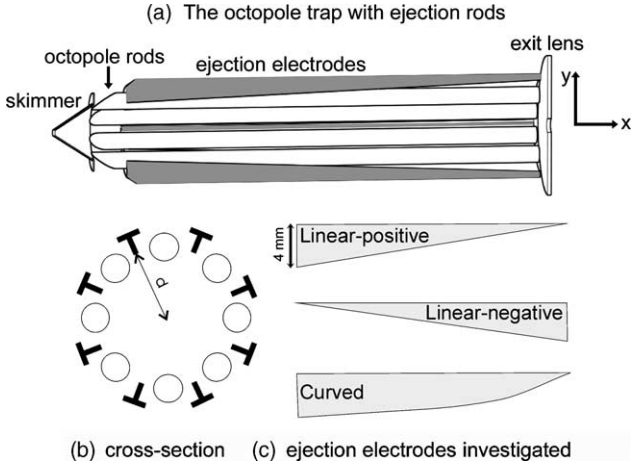

Fig. 1. (a) The ion source includes a skimmer, an accumulation octopole with ejection electrodes and an exit lens, l_e, (b) Cross-section of the accumulation octopole including the T-shaped ejection electrodes (at the deepest point of the stem $d = 11.6$ mm) and (c) longitudinal view of the three ejection electrodes reported here.

provide the axial trapping field for the ions. Fig. 1 shows a schematic of the octopole design.

Various T-shaped electrodes placed between the octopole rods were investigated. Here, the evaluations of three electrode geometries are reported. These are shown in Fig. 1c and are:

(i) Linear-positive—the stem is initially 4 mm and decreases linearly with distance to 0 mm at the end of the octopole.
(ii) Linear-negative—the stem is initially 0 mm and increases linearly with distance to 4 mm at the end of the octopole.
(iii) Curved—the stem of the T-shaped electrode is initially 4 mm and decreases in size non-linearly to zero.

The thickness of the steam is 1 mm in all situations. The two linear electrode configurations produce a non-linear ejection field, whereas the curved electrodes were designed to produce a linear ejection field. An ejection field for positive ions is produced by applying a positive potential to the linear-positive and curved ejection electrode geometries whereas a negative-potential is required for the linear-negative geometry.

3. SIMION simulations

The purpose of this work was to approximate a collisionally cooled ion beam that is trapped in a long octopole ion trap and to investigate the effects of axial ejection fields on the time and energy distributions of the ejected ion packets. These analyses were performed using SIMION 7.0 [33]. The scaling used in the SIMION simulations of the octopole was five grid units per mm (gu/mm).

The simulation results reported here pertain only to the analysis of low abundant ions: under conditions of high space charge the ejection field will be effectively screened by the ion-cloud. Moreover, improvements in sensitivity are not required for intense ion currents. In addition, SIMION does not approximate space-charge particularly well and cannot run the groups of ions required for its space-approximations in a radio frequency device in a practical time. For these reasons, ion–ion interactions were not taken into account. These simulations were performed specifically to increase the sensitivity for the analysis of low abundance ions, to trap and transfer these ions to the ICR cell as efficiently as possible; those experiments that require improvements in efficiency and that are best described by the simulation constraints.

Ions of mass equal to that of cytochrome *c*, 12,360 Da, and with charges of +1 and +15 were used in the simulations. To approximate the ion beam emitted through the skimmer of an electrospray ion source, the initial positions, angles and times of the incoming ions were randomized through the ranges $0 \leq [y, z] \leq 0.5$ mm, $0 \leq \theta \leq 2^\circ$, $0 \leq t \leq 4$ ms with an initial energy of 10 eV for +15 ions and 3 eV for singly charged ions. Note the initial energy of the ions has no effect for the evaluation of the ejection time and energy distributions because the ions are thermalized prior to the ejection pulse. For each set of parameters 1000 cytochrome *c* ions were initiated at the beginning of the accumulation octopole. The radio-frequency voltage used for these simulations was 800 V peak-to-peak and the frequency was 0.88 MHz. This voltage was sufficient to trap ions with $m/z = 12{,}360$, but lower voltages can be used for a smaller m/z range.

An accumulation–ejection pulse sequence, which involves the skimmer, the dc ejection electrodes, and the exit lens, is shown in Fig. 2. The ions were accumulated for 14 ms (thermalized) using 5 V applied to the skimmer and 10 V to the exit lens and 0 V to the ejection electrodes. To eject ions 150 V was applied to the skimmer, −1 V to the exit lens and 200 V to the ejection electrodes (−200 V for the linear negative configuration).

The hard spheres algorithm [30] was used in order to estimate the collisional cooling in the simulations, using the cross-section of cytochrome *c* determined from ion mobility spectrometry. The cross-section of gas phase cytochrome *c* has been shown to be charge dependent [34].

This algorithm is an approximation of ion–molecule collisions that is valid for the range of kinetic energies present here. Collisional relaxation from the initial velocity to the thermal equilibrium velocity follows the law:

$$v = v_0 \, \mathrm{e}^{-t/\tau} \tag{1}$$

Here, v_0 is the initial velocity of the ion, v the velocity at a time t, and τ corresponds to the relaxation time, defined by formula:

$$\tau = 3(m + m_g)/4 m_g n \sigma u_{kT}, \qquad u_{kT} = (8kT/\pi m_r)^{1/2} \tag{2}$$

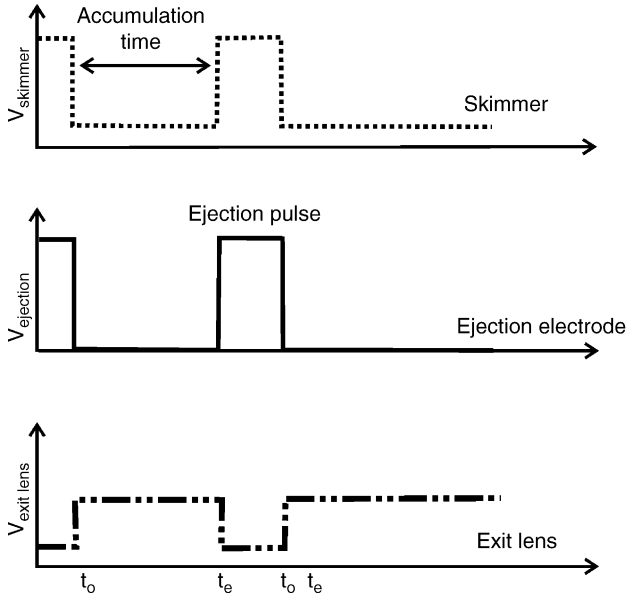

Fig. 2. Accumulation–ejection pulse sequence used for accumulation and ejection of ions. The difference t_e (ejection) − t_0 (accumulation) represents the accumulation time. A new cycle starts at the time $t = t_0'$. The rf voltage is applied throughout simulations. $V_{\text{skimmer accum}} = 5$ V, $V_{\text{skimmer ejec}} = 150$ V, $V_{\text{exit lens accum}} = 10$ V, $V_{\text{exit lens ejec}} = -1$ V, $V_{\text{eject electrodes accum}} = 0$ V, $V_{\text{eject electrodes ejec}} = 200$ V.

where m_r is the reduced mass ($m_r = mm_g/(m + m_g)$), T the temperature of the collision gas and k the Boltzmann constant, n is the number density of the gas molecules and σ is the collisional cross-section. m and m_g represent the mass of the ion, and the mass of the collision gas, respectively. Using a pressure of 10^{-3} mbar throughout the simulated octopole, the relaxation times were calculated to be 2.5 and 1.1 ms for +1 and +15 ions, respectively. These were implemented in SIMION through a user program that damps the ion's velocity according to the above equation but does not modify the instantaneous direction of the ions. For the pressure assumed here and the large cross-section of the analyte ions, such viscous damping is a good approximation of the large number of collisions experienced by each ion.

This simulation of an accumulation octopole enables a qualitative assessment of the performance of an octopole with ejection electrodes for the accumulation and ejection of low abundant ions. In agreement with the simulations preliminary experimental results demonstrate the higher sensitivity of this new octopole when voltage is applied to the dc ejection electrodes and an axial ejection field is generated.

4. Results and discussion

The time and energy distributions of the ions ejected from the octopole are compared for the three configurations shown in Fig. 1c and for an octopole without an axial field. These distributions were recorded at the exit of the octopole and at the FTICR entrance (quadrupole ion guides transport ions from the octopole exit to the cell, see Fig. 3; more details can be found in reference [35]). All three octopole configurations transported ions covering a wide m/z range with high efficiency (100%), thus demonstrating that the ejection electrodes do not significantly distort the rf field of the octopole (results not shown). Note that the ion transmission through the exit lens depends on the voltage applied to the exit lens and the size of the aperture.

Fig. 4a shows the axial dc potential gradient of the linear-positive and linear-negative designs (0 V applied to the octopole electrodes). As can be seen, the axial field is very steep in the areas influenced by the skimmer and the exit lens potentials. Between the skimmer and the exit lens the dc ejection electrodes of both configurations provide an average axial potential gradient of 0.3 V/cm (non-linear) along the octopole when 200 V is applied to the dc ejection electrodes. This potential gradient has been shown to be optimum for a segmented quadrupole linear ion trap that was used to accumulate ions for FTICR experiments, larger ejection fields decreasing sensitivity [15]. Closer examination of Fig. 4a reveals that the linear-negative configuration has a shallow potential gradient at the beginning of the octopole and a steeper potential gradient at the exit (in the region without influence from the skimmer and the exit lens). This profile

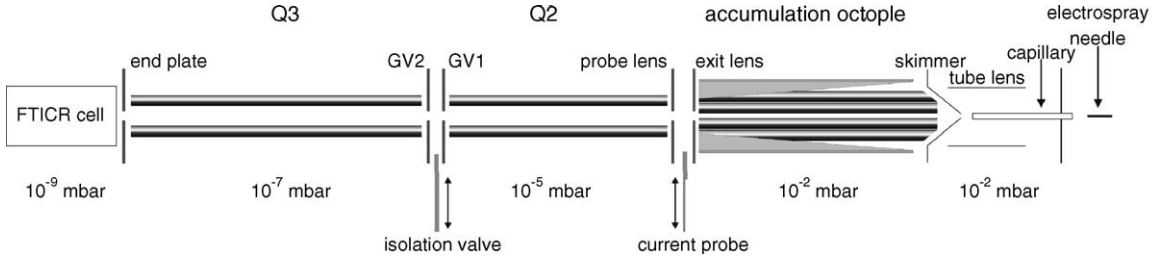

Fig. 3. Schematic of the 7 T external electrospray FT-ICR set-up. The accumulation octopole, the following two quadrupoles and the lenses located at the entrance and exit of the multipoles were simulated using two potential arrays. A higher resolution array, 5 gu/mm, was used to model the accumulation octopole and a lower resolution array, 2 gu/mm, was used to model the two transfer quadrupoles and transfer lenses. The two arrays were joined in the middle of the exit lens, where the field lines are almost linear, and using identical potentials on the exit lens in both arrays. Due to low pressures no damping of the velocity is considered in the transfer quadrupoles. The voltages applied to the transfer optics and the two quadrupoles are: $V_{\text{pp Q2,3}} = 200$ V, $V_{\text{probe lense}} = -2$ V, $V_{\text{GV1}} = -20$ V, $V_{\text{GV2}} = -70$ V, $V_{\text{end plate}} = -1$ V, $V_{\text{bias Q2}} = -2$ V, $V_{\text{bias Q3}} = -1$ V.

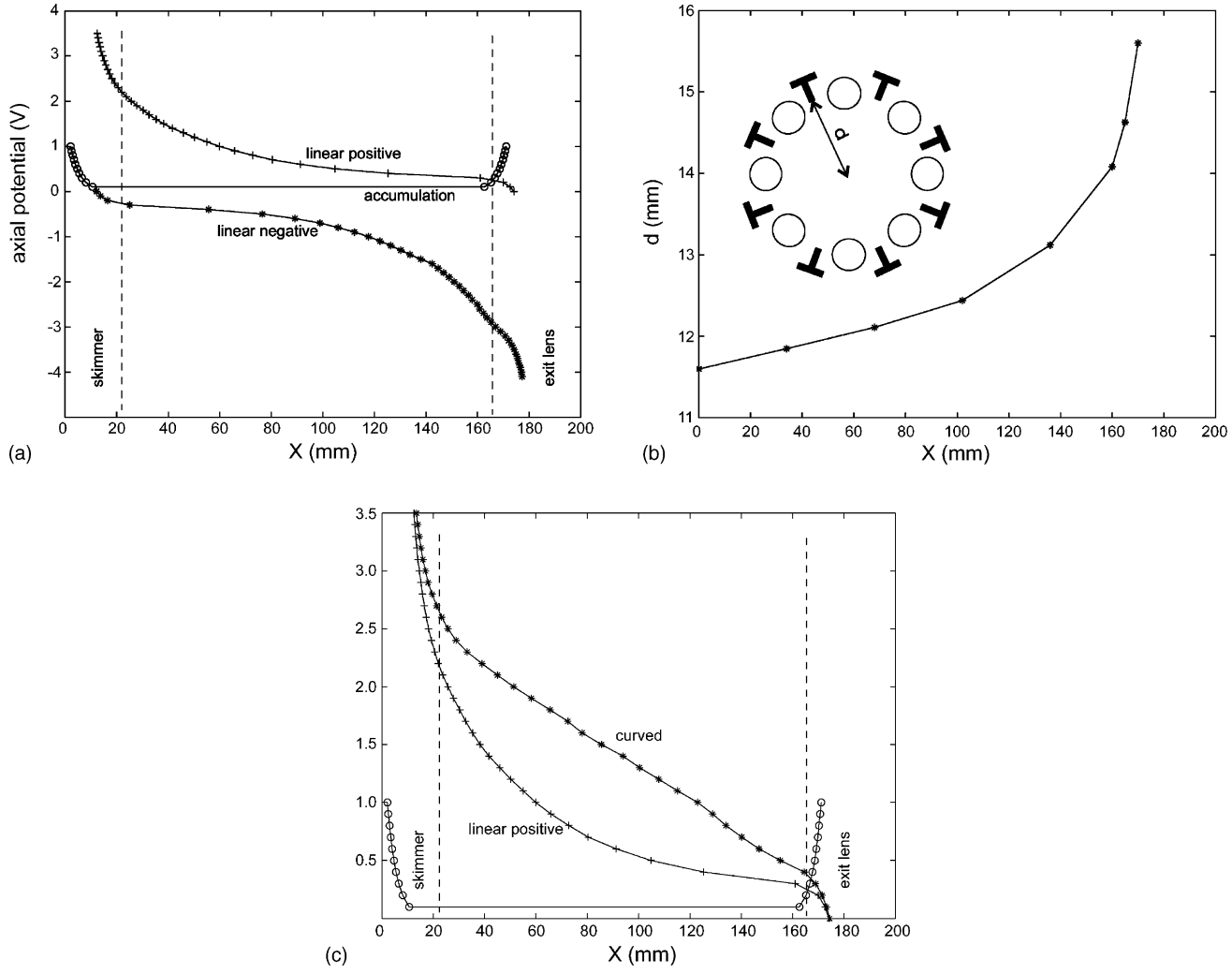

Fig. 4. The axial dc potential along the accumulation octopoles working in ejection mode for: (a) linear-positive (+) and linear-negative (*) configurations; (b) the variation of the dc election electrode stem length *d* from the beginning to the end of the octupole; (c) linear-positive (+) and curved (*) configurations. The potential profile during accumulation is the same for all three configurations (◯). The dashed lines show the place where the field of the skimmer and the exit lens effect the axial potential during the ejection time. During accumulation V_{skimmer} = 5 V, $V_{\text{exit lens}}$ = 10 V and $V_{\text{eject electrodes}}$ = 0 V. During ejection V_{skimmer} = 150 V, $V_{\text{exit lens}}$ = −1 V and $V_{\text{eject electrodes}}$ = 200 V for the linear-positive ejection electrodes and V_{skimmer} = 5 V, $V_{\text{exit lens}}$ = −5 V and $V_{\text{eject electrodes}}$ = −200 V for the linear negative design.

will cause the ions located near the beginning of the octopole to be accelerated more slowly than those located near the end, a profile not favorable for a narrow time spread.

In order to investigate the performance of a linear ejection field, curved ejection electrodes were designed. The field at the center of the octopole was measured as a function of the stem length of the ejection electrode; the stem length was then varied along the length of the ejection electrodes such that a linear ejection field was produced. Fig. 4b shows the dimensions of these curved ejection electrodes.

Fig. 4c shows the axial potential profiles for the curved and linear-positive geometries, resulting in linear and non-linear axial potential gradients, respectively. Energy and time distributions were recorded at the exit of the accumulation octopole for the curved and linear-positive configurations and without an axial field ($V_{\text{dc electrode}}$ = 0 V).

Fig. 5 shows the time and energy distributions for *z* = +15 cytochrome *c* ions at the octopole exit. The ejection time spread was almost identical for the curved and linear-positive ejection electrodes (approximately 0.23 ms), whereas without an axial field the time spread was much larger, 12 ms. The time spread of 0.23 ms corresponds to approximately 3 V, *z* = +15 ions moving across the 180 mm length of the octopole. The analogous time spread for the singly charged ions was approximately 0.88 ms with the ejection field and 22.64 ms without the ejection field (results not shown). Though larger energies (22–43 or 1.5–2.9 eV per charge) were obtained for the curved ejection electrodes than for the linear-positive configuration (19–36 eV, or 1.3–2.4 eV per charge), both energy ranges can be accommodated by the FTICR cell. However, closer examination of the energy–time distribution of the linear positive configuration reveals that

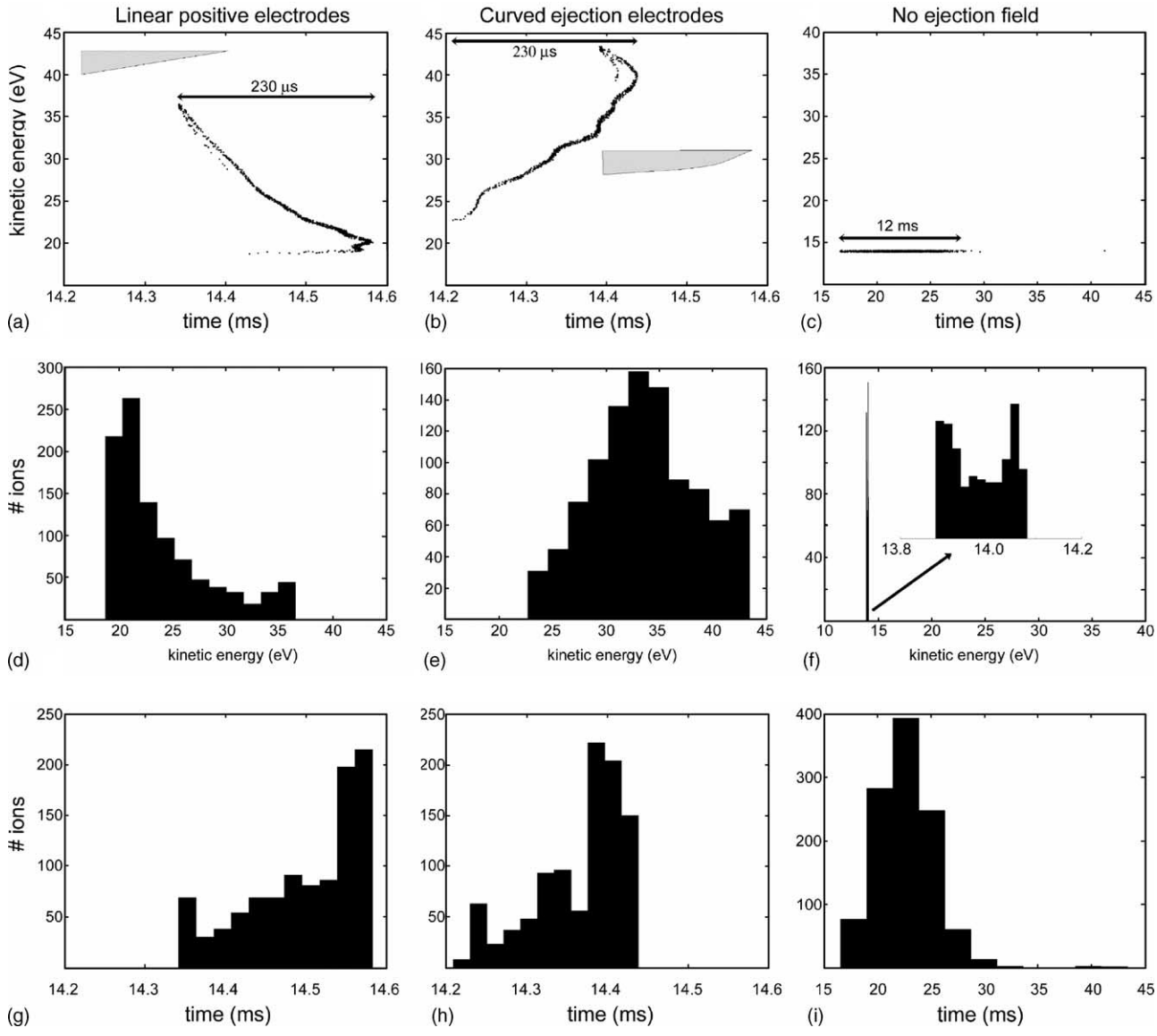

Fig. 5. Time and energy distributions of the ion packet at the exit lens of the octopole ($z = +15$ ion). The first column shows a scatter plot of the time and kinetic energy distributions, and histograms of the kinetic energy distribution (middle) and the time distribution (bottom), for the ion packet ejected from the linear positive ejection electrodes configuration. The second and third columns show the results obtained for the curved electrode configuration, and with no axial field. Ions are accumulated 14 ms and then ejected. Only the period of ejection is shown in this figure ($t = 0$ is defined as the time when ions enter the octopole).

the ions that are ejected first have the highest energy. The ions located at the beginning of the octopole experience a larger ejection field and have overtaken the ions located closer to the exit. Fig. 5 also shows the corresponding time and energy histograms. It can be seen that more ions with lower kinetic energies were ejected by the linear-positive configuration than with the curved configuration. The energy distribution from the octopole without an axial field is much narrower, but has the drawback of a much larger time spread. Note the time spread is not thermal because the times were recorded after the ions have been ejected from the octopole and passed through the −1 V field of the exit lens.

Simulations of the entire ion transfer system, two quadrupole ion guides and electrostatic lenses (Fig. 3), were used to determine the time and energy distributions at the entrance of the FTICR cell. These results can be seen in Fig. 6. Because the ions with higher energy had overtaken those with lower energy for the linear-positive configuration, the time spread encompassing the majority of the $z = +15$ ions (90%) at the entrance of the cell is larger than that for the curved configuration (1.17 and 0.77 ms, respectively). The mean and the width of the kinetic energy distributions were smaller for the linear-positive configuration, but the time spread was smaller for the curved ejection electrodes configuration at the FTICR entrance (i.e., better bunching).

Due to the short trapping time window of the cell a more compact ion cloud at the entrance to the FTICR cell will lead to more efficient trapping, thus increased sensitivity. For

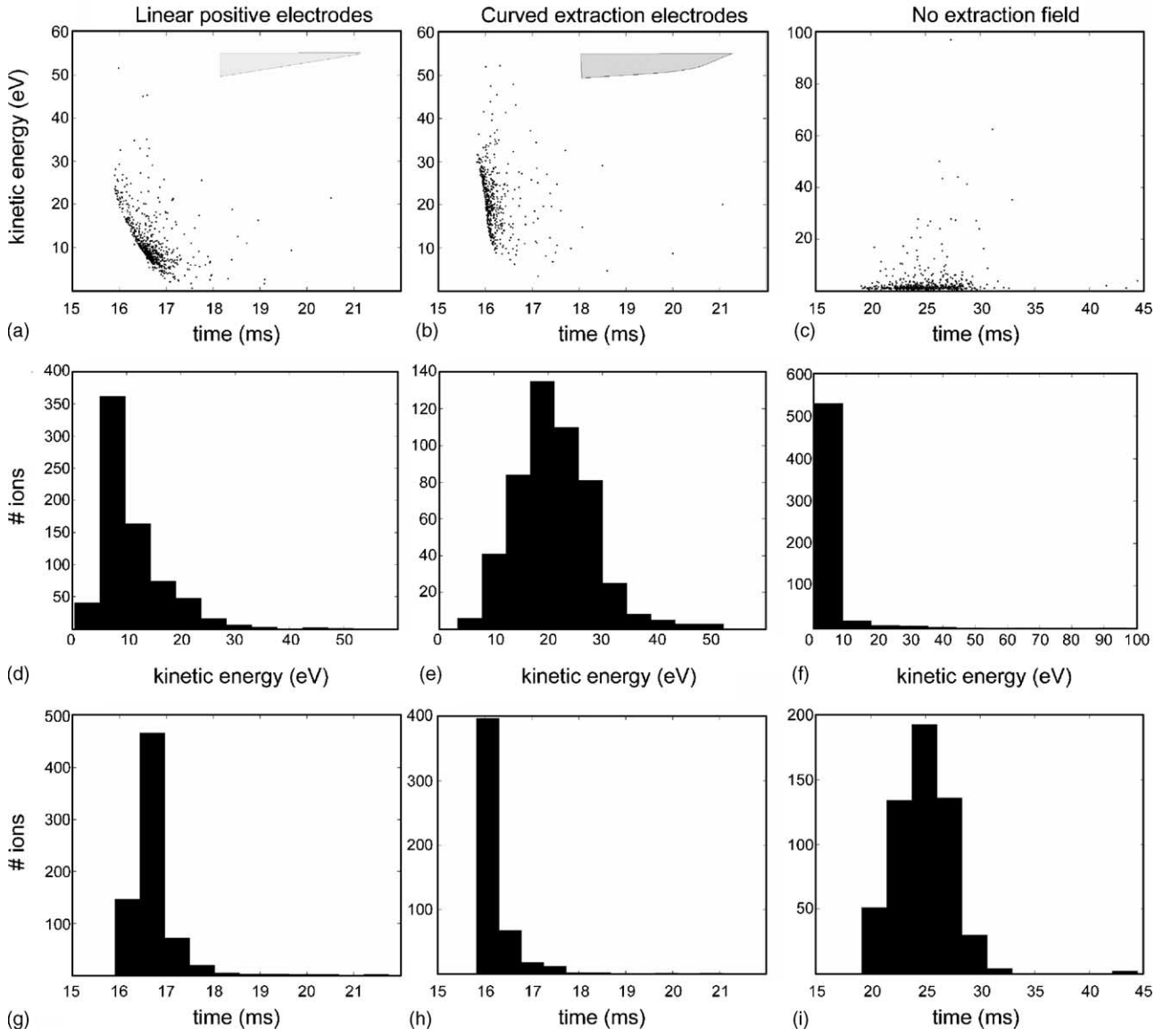

Fig. 6. Time and energy distributions of the ion packet at the entrance of the ICR cell ($z = +15$ ion). The first column shows a scatter plot of the time and kinetic energy distributions, and histograms of the kinetic energy distribution (middle) and the time distribution (bottom), for the ion packet ejected from the linear positive ejection electrodes configuration. The second and third columns show the results obtained for the curved electrode configuration, and with no axial field. Only the period of ejection is shown in this figure ($t = 0$ is defined as the time when ions enter the octopole).

both axial potential configurations the ion energy was within the acceptable limits thus the octopole that gave a shorter trapping time spread is considered to be the better choice. Again, without an axial ejection field the time spread is too large for efficient transfer and trapping of the ions in the FTICR cell (Fig. 6).

An estimate of the increase in sensitivity for +15 cytochrome *c* ion, $m/z = 824$, was made by comparing the maximum density of ions at the cell in the time distributions of the curved- and no-ejection electrode configurations, and a trapping window of 0.2–0.4 ms. The octopole with the curved ejection electrodes was estimated to be 4–5 times more sensitive because of improved time-focusing at the FTICR cell.

Fig. 7 shows preliminary experimental results obtained with an accumulation octopole of the curved electrode configuration. The ions generated from electrospray ionization of 5 μM cytochrome *c* in 69:29:2 methanol:water:acetic acid were accumulated in the octopole for 0.4 s before being transferred to the ICR cell for detection. As can be seen, the signal intensities with the ejection field, upper spectrum, were approximately 100% stronger than that with no ejection field (0 V applied to ejection electrodes, bottom figure). Furthermore, these sensitivity improvements were observed for several charge states of cytochrome *c* indicating that sensitivity improvements can be made over *m*/*z* ranges compatible with LC–MS experiments of low abundance peptides, the application of interest. It also

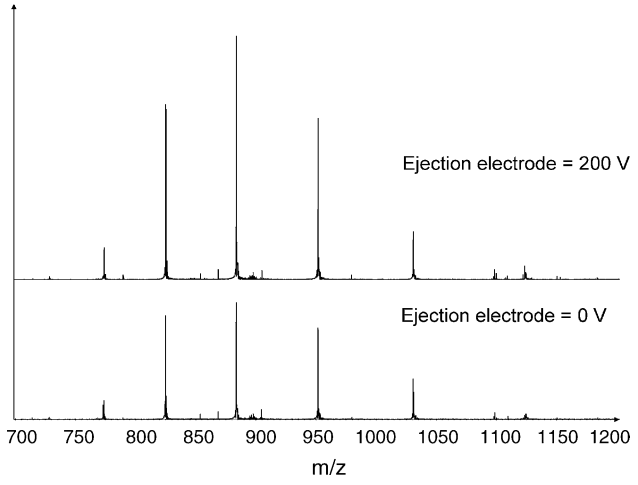

Fig. 7. Experimental mass spectra of cytochrome *c* when 200 V (upper figure) and 0 V (lower figure) where applied to the ejection electrodes of the curved configuration. The arbitrary *y*-scales on both figures are identical.

demonstrates that the time-of-flight effects of external trap FTICR experiments [11], which will be more pronounced with time-focused ejection, do not overwhelm the sensitivity gains from time-focusing of the ejected ions.

Before concluding it is pertinent to question why the experimentally measured improvement in sensitivity was less than that estimated using the simulations. The simulations represent an approximation of a real octopole ion trap. Uniform pressure throughout the octopole and negligible space charge effects are arguably the two most important. The pressure in an ESI experiment is not uniform. Fig. 3 shows that the octopole ion trap is the second stage of a differentially pumped apparatus. Consequently a pressure gradient will exist along the length of the trap. Higher pressures at the beginning of the octopole will lead to greater viscous damping that can hinder ion ejection. This effect would increase the time spread of the ejected ions and thus decrease the available sensitivity gains.

As explained in the section describing the simulations, ion–ion interactions were not included for practical and reliability reasons. Space charge can shield the ions from the ejection field (higher space charge leads to a less effective the ejection field), thus reducing the time focusing at the FTICR cell and the sensitivity gains obtained. Additionally, high space charge increases the radial size of the ion cloud in the octopole. Consequently, fewer ions might be transferred through the exit lens of the octopole accumulation device. The simulations showed that 70% of the $m/z = 12{,}360$ ($z = +1$) passed through the exit lens with a 4 mm diameter hole but 100% of the $m/z = 824$ ($z = +15$) because ions of larger m/z ($m/z = 12{,}360$) are less radially confined by the rf field of the octopole than ions of smaller m/z [30,36]. Space charge will broaden the cloud even more [36], resulting in less confined ion beams, so lowering the sensitivity compared to simulations.

The lower (but still significant) sensitivity gains of the preliminary experimental results, with respect to the simulation estimation, could reflect the pressure gradient across the octopole and/or space charge effects. While the latter will be diminished for ions of low intensity, the application of interest, an improved understanding of the physics of ion accumulation and transfer to the ICR cell could enable further sensitivity gains to be attained.

5. Conclusions

Here, we have used simulations to investigate a long octopole ion trap that either has an axial potential gradient or no axial potential gradient for external accumulation and efficient transfer of ions to an FTICR-MS analyser cell. The time and energy distribution of the ions at the exit of the octopole and at the entrance of the cell show that the octopole with curved ejection electrodes (linear axial field) lead to higher sensitivity, 400–500%. Preliminary experimental results showed that these ejection electrodes increased the ion signal from electrospray ionisation of cytochrome *c* by approximately 100% and that sensitivity improvements spanned an m/z range compatible the LC–MS of complex peptide solutions. The different degree of improvement between the simulations and preliminary experiments is most likely due to the approximations inherent to the simulations and will be the subject of a future experimental investigation.

Acknowledgements

This work is part of the research program of the “Stichting voor Fundamenteel Onderzoek der Materie (FOM)”, which is financially supported by the “Nederlandse organisatie voor Wetenschappelijk Onderzoek (NWO)”. The authors also wish to thank Bruker Daltonics and Netherlands Proteomics Centre (NPC) for generous financial support.

References

[1] J. Bergquist, M. Palmblad, M. Wetterhall, P. Håkansson, K. Markides, Mass Spectrom. Rev. 21 (2002) 2.
[2] T.P. Conrads, K. Alving, T.D. Veenstra, M.E. Belov, G.A. Anderson, D.J. Anderson, M.S. Lipton, L. Paša-Tolicǐ, H.R. Udseth, W.B. Chrisler, B.D. Thrall, R.D. Smith, Anal. Chem. 73 (2001) 2132;
L. Paša-Tolicǐ, M.S. Lipton, C.D. Masselon, G.A. Anderson, Y. Shen, N. Tolicǐ, R.D. Smith, J. Mass Spectrom. 37 (2002) 1185.
[3] Y. Shen, N. Tolic’, R. Zhao, L. Paša-Tolicǐ, L. Li, S.J. Berger, R. Harkewicz, G.A. Anderson, M.E. Belov, R.D. Smith, Anal. Chem. 73 (2001) 3011.
[4] R.D. Smith, Int. J. Mass Spectrom. 200 (2000) 509.
[5] M.R. Emmet, F.M. White, C.L. Hendrickson, S.D.-H. Shi, A.G. Marshall, J. Am. Soc. Mass Spectrom. 9 (1998) 333;
C. Ihling, K. Berger, M.M. Höfliger, D. Führer, A.G. Beck-Sickinger, A. Sinz, Rapid Comm. Mass Spectrom. 17 (2003) 1240;
M. Palmblad, Y.O. Tysbin, M. Ramström, J. Bergquist, P. Håkansson, Rapid Comm. Mass Spectrom. 16 (2002) 988;

T.L. Quenzer, M.R. Emmett, C.L. Hendrickson, P.H. Kelly, A.G. Marshall, Anal. Chem. 73 (2001) 1721.
[6] P.K. Jensen, L. Paša-Tolic', G.A. Anderson, J.A. Horner, M.S. Lipton, J.E. Bruce, R.D. Smith, Anal. Chem. 71 (1999) 2076.
[7] M.B. Comisarow, A.G. Marshall, Chem. Phys. Lett. 26 (1974) 489.
[8] F. He, C.L. Hendrickson, A.G. Marshall, Anal. Chem. 73 (2001) 647.
[9] K. Miyabayashi, Y. Naito, M. Miyake, K. Tsujimoto, Eur. J. Mass Spectrom. 6 (2000) 251;
C.A. Hughey, R.P. Rodgers, A.G. Marshall, Anal. Chem. 74 (2002) 4145;
L.A. McDonnell, P.J. Derrick, B.B. Powell, P. Double, Eur. J. Mass Spectrom. 9 (2003) 117;
D.J. Aaserud, L. Prokai, W.J. Simonsick Jr., Anal. Chem. 71 (1999) 4793.
[10] P. Caravatti, M. Allemann, Org. Mass Spectrom. 26 (1991) 514.
[11] P.B. O'Conner, M. Duursma, G.J.V. Rooij, R.M.A. Heeren, J. Boon, J., Anal. Chem. 69 (1997) 2751.
[12] A.M. Hawkridge, L. Zhou, M.L. Lee, D.C. Muddiman, Anal. Chem. 76 (2004) 4118;
M.E. Belov, M.V. Gorshkov, H.R. Udseth, G.A. Anderson, A.V. Tolmachev, D.C. Prior, R. Harkewicz, R.D. Smith, J. Am. Soc. Mass Spectrom. 11 (2000) 19;
A.W. Colburn, A.E. Giannakopulos, P.J. Derrick, Eur. J. Mass Spectrom. 10 (2004) 149;
P.B. O'Connor, Rapid Comm. Mass Spectrom. 16 (2002) 1160;
A.G. Marshall, Int. J. Mass Spectrom. 200 (2000) 331;
M.E. Belov, R. Zhang, E.F. Strittmatter, D.C. Prior, K. Tang, R.D. Smith, Anal. Chem. 75 (2003) 4195.
[13] M.E. Belov, M.V. Gorshkov, H.R. Udseth, G.A. Anderson, R.D. Smith, Anal. Chem. 72 (2000) 2271.
[14] A. Dodonov, V. Kozlovsky, A. Loboda, V. Raznikov, I. Sulimenkov, A. Tolmachev, A. Kraft, H. Wollnik, Rapid Comm. Mass Spectrom. 11 (1997) 1649.
[15] M.E. Belov, E.N. Nikolaev, G.A. Anderson, H.R. Udseth, T.P. Conrads, T.D. Veenstra, C.D. Masselon, M.V. Gorshkov, R.D. Smith, Anal. Chem. 73 (2001) 253.
[16] J.M. Campbell, B.A. Collings, D.J. Douglas, Rapid Comm. Mass Spectrom. 12 (1998) 1463;
M.W. Senko, C.L. Hendrickson, M.R. Emmett, S.D.H. Shi, A.G. Marshall, J. Am. Soc. Mass Spectrom. 8 (1997) 970.
[17] B. Cha, M. Blades, D.J. Douglas, Anal. Chem. 72 (2000) 5647;
Y. Huang, S. Guan, H.S. Kim, A.G. Marshall, Int. J. Mass Spectrom. Ion Proc. 152 (1996) 121;
A. Kellerbauer, T. Kim, R.B. Moore, P. Varfalvy, Nucl. Instr. Meth. A 469 (2001) 276;
A.N. Krutchinsky, I.V. Chernushevich, V.L. Spicer, W. Ens, K.G. Standing, J. Am. Soc. Mass Spectrom. 9 (1998) 569;
P.A. Limbach, A.G. Marshall, M. Wang, Int. J. Mass Spectrom. Ion Proc. 125 (1993) 135;
M.D. Lunney, R.B. Moore, Int. J. Mass Spectrom. Ion Proc. 190/191 (1999) 153;
R.T. McIver Jr., R.L. Hunter, W.D. Bowers, Int. J. Mass Spectrom. Ion Proc. 64 (1985) 67;
A.V. Tolmachev, I.V. Chernushevich, A.F. Dodonov, K.G. Standing, Nucl. Instr. Meth. A 124 (1997) 112;
R.D. Voyksner, H. Lee, Rapid Comm. Mass Spectrom. 13 (1999) 1427;
Y. Wang, S.D.H. SHi, C.L. Hendrickson, A.G. Marshall, Int. J. Mass Spectrom. 198 (2000) 113.
[18] M.E. Belov, E.N. Nikolaev, K. Alving, R.D. Smith, Rapid Comm. Mass Spectrom. 15 (2001) 1172.
[19] K. Håkansson, J. Axelsson, M. Palmblad, P. Håkansson, J. Am. Soc. Mass Spectrom. 11 (2000) 210.
[20] L.A. McDonnell, A.E. Giannakopulos, P.J. Derrick, Y.O. Tsybin, P. Håkansson, Eur. J. Mass Spectrom. 8 (2002) 181;
K. Sannes-Lowery, R.H. Griffey, G.H. Kruppa, S.J. P, S.A. Hofstadler, Rapid Comm. Mass Spectrom. 12 (1998) 1957;
K.A. Sannes-Lowery, S.A. Hofstadler, J. Am. Soc. Mass Spectrom. 11 (2000) 1.
[21] I.V. Chernushevich, B.A. Thomson, Anal. Chem. 76 (2004) 1754.
[22] A. Loboda, A. Krutchinsky, O. Loboda, J. McNabb, V. Spicer, W. Ens, K. Standing, Eur. J. Mass Spectrom. 6 (2000) 541.
[23] F. Herfurth, J. Dilling, A. Kellerbauer, G. Bollen, S. Henry, H.-J. Kluge, E. Lamour, D. Lunney, R.B. Mooore, C. Scheidenberger, S. Schwarz, G. Sikler, J. Szerypo, Nucl. Instr. Meth. A 469 (2001) 254.
[24] B. Thomson, C. Jolliffe, R. Javahery, Proceedings of the 44th ASMS Conf. Mass Spectrom. and Allied Topics, Portland, USA, 1996.
[25] B.A. Mansoori, E.W. Dyer, C.M. Lock, K. Bateman, R.K. Boyd, B.A. Thomson, J. Am. Soc. Mass Spectrom. 9 (1998) 775.
[26] B.E. Wilcox, C.L. Hendrickson, A.G. Marshall, J. Am. Soc. Mass Spectrom. 13 (2002) 1304.
[27] J.B. Fenn, M. Mann, C.K. Meng, S.F. Wong, C.M. Whitehouse, Science 246 (1989) 64.
[28] M. Karas, D. Bachmann, U. Bahr, F. Hillenkamp, Int. J. Mass Spectrom. Ion Process. 78 (1987) 53.
[29] C. Hägg, I. Szabo, Int. J. Mass Spectrom. Ion Proc. 73 (1986) 295.
[30] A.V. Tolmachev, H.R. Udseth, R.D. Smith, Int. J. Mass Spectrom. 222 (2003) 155.
[31] Dawson, P.H. Quadrupole mass spectrometry and its applications: New York, 1976.
[32] V.V.K. Rama Rao, A. Bhutani, Int. J. Mass Spectrom. 202 (2000) 31.
[33] D.A. Dahl, Int. J. Mass Spectrom. 200 (2000) 3.
[34] M.F. Jarrold, Annu. Rev. Phys. Chem. 51 (2000) 179.
[35] A. Römpp, R. Mihalca, M.C. Duursma, T.H. Mize, L.A. McDonnell, R.M.A. Heeren, Eur. J. Mass Spectrom. (2005) in press.
[36] A.V. Tolmachev, H.R. Udseth, R.D. Smith, Rapid Comm. Mass Spectrom. 14 (2000) 1907.